JBC Papers in Press. Published on March 13, 2019 as Manuscript RA119.007653
The latest version is at http://www.jbc.org/cgi/doi/10.1074/jbc.RA119.007653

NMR- and MD simulation–based structural characterization of the membrane-associating FATC domain of ataxia telangiectasia mutated

Munirah S. Abd Rahim[1], Yevhen K. Cherniavskyi[2], D. Peter Tieleman[2], Sonja A. Dames[1,3$]

From the [1]Chair of Biomolecular NMR Spectroscopy, Department of Chemistry, Technische Universität München, Lichtenbergstr. 4, 85747 Garching, Germany, [2]Department of Biological Sciences and Centre for Molecular Simulation, University of Calgary, Calgary, AB, Canada, [3]Institute of Structural Biology, Helmholtz Zentrum München, Ingolstädter Landstr. 1, 85764 Neuherberg, Germany

Running title: Structure of membrane-associating ATM FATC

[$]To whom correspondence may be addressed: Chair of Biomolecular NMR Spectroscopy, Department of Chemistry, Technische Universität München, Lichtenbergstr. 4, 85747 Garching, Germany, Tel.: +49-89-35831-7103, Fax: +49-89-3229-4002, E-mail: (sonja.dames@tum.de)

Keywords: Ataxia telangiectasia mutated, phosphatidylinositol 3-kinase related kinase, protein membrane interactions, signaling at membranes, NMR, MD simulations, structural dynamics, FATC domain, solution structure

ABSTRACT

The Ser/Thr protein kinase ataxia telangiectasia mutated (ATM) plays an important role in the DNA damage response, signaling in response to redox signals, the control of metabolic processes, and mitochondrial homeostasis. ATM localizes to the nucleus and at the plasma membrane, mitochondria, peroxisomes, and other cytoplasmic vesicular structures. It has been shown that the C-terminal FATC domain of human ATM (hATMfatc) can interact with a range of membrane mimetics and may thereby act as a membrane-anchoring unit. Here, NMR structural and ^{15}N-relaxation data, NMR data using spin-labeled micelles, and MD simulations of micelle-associated hATMfatc revealed that it binds the micelle by a dynamic assembly of three helices with many residues of hATMfatc located in the head-group region. We observed that none of the three helices penetrates the micelle deeply or makes significant tertiary contacts to the other helices. NMR-monitored interaction experiments with hATMfatc variants in which two conserved aromatic residues (Phe-93 and Trp-96) were either individually or both replaced by alanine disclosed that the double substitution does not abrogate the interaction with micelles and bicelles at the high concentrations these aggregates are typically used, but impairs interactions with small unilamellar vesicles (SUVs), usually used at much lower lipid concentrations and considered a better mimetic for natural membranes. We conclude that the observed dynamic structure of micelle-associated hATMfatc may enable it to interact with differently composed membranes or membrane-associated interaction partners and thereby regulate ATM's kinase activity. Moreover, the FATC domain of ATM maybe function as membrane-anchoring unit for other biomolecules.

Ataxia telangiectasia mutated (ATM) belongs to the family of phosphatidylinositol 3-kinase related kinases (PIKKs) that phosphorylate Ser/Thr residues of proteins regulating processes such as DNA repair,

cell cycle progression, cellular senescence, apoptosis, and metabolic processes (1-4). Recently, it became further aware that PIKKs also play a role in signaling in response to virus infections and during inflammation (5,6). The function of ATM and of the related mammalian/mechanistic target of rapamycin (mTOR), a central controller of cell growth and metabolism in all eukaryotes that also has links to DNA repair signaling (7,8), has further been related to redox signaling (9-12). Whereas the mTOR pathway negatively controls ATM (13), ATM inactivates mTORC1 in response to reactive oxygen species (ROS) to induce autophagy (12), apparently rather selectively that of peroxisomes (14). ATM also downregulates mTORC1 under hypoxic conditions (11). Other studies support that ATM plays direct roles in modulating mitochondrial homeostasis (15). Activation of ATM by oxidation and other factors has been reviewed (16). Inactivation of ATM leads to Ataxia-Telangiectasia (A-T) disease and more generally plays a role in neuronal development and neurodegeneration (17). Because ATM controls different signaling pathways important for the DNA damage response, cell cycle check points and metabolic processes, it is considered an interesting therapeutic target with respect to cancer (18).

It has been proposed that targeted membrane localization allows spatial separation of individual signaling branches of large signaling networks, thereby potentially improving the reliability of biochemical signaling processes (19). Since PIKKS generally participate in a multitude of signaling pathways in response to ionizing radiation and other stress factors or metabolic signals (2,5,7,16,20,21), their localization may also determine the specific signaling output (22). ATM has not only been found to localize and function in the nucleus but also in the cytoplasm (12). ATM has further been localized at microsomes (23) and cytoplasmic vesicles (24), as well as at membrane-associated vesicles (25). More recently, it has been reported that PEX5 peroxisome import receptor binds ATM to localize it to peroxisomes and that ATM can localize to mitochondria (14,15).

Although the total length of PIKK amino acid sequences ranges from about 2500 to 4500 residues, all share a similar domain organization (5,22). Fig. 1A shows human ATM as representative example. The Ser/Thr kinase domain is close to the C-terminus and shows homology to lipid kinases (4). Except for TRRAP, all are catalytically active (1,4). The FRAP-ATM-TRRAP (FAT) domain resides N-terminal of the kinase (22,26). Based on sequence analysis the FAT and the preceding N-terminal region with only low sequence similarity between different PIKKs are mostly composed of α-helical repeat motifs that typically form platforms for protein-protein interactions (26-28). The linker region between the kinase and the FAT C-terminal (FATC) domain region varies significantly in length and sequence composition (4,29). It has been referred to as PIKK regulatory domain (PRD) (1,4,29). The highly evolutionary conserved region of the FATC domain is made up by the ~35 C-terminal residues (PFAM domain database entry PF02660) (4,26,30-32). Based on mutagenesis studies and other data, this domain generally plays an important role for the regulation of PIKK function (4,29,31,33-35).

Obtaining high-resolution structural data for PIKKs is challenging due to their large size. For ATM electron microscopy (EM) structural data at lower resolution provided insights in the interaction with DNA (36), the inhibitory effect of dimerization of human ATM (37), and the dimerization properties of the yeast ATM homolog Tel1 (38,39). In 2017, higher resolution EM structures of the closed ATM dimer (PDB-ID 5NP0, 5.7 Å resolution) and the presumably more active open ATM dimer (PDB-ID 5NP1, 5.7 Å resolution for combined data) were published (40).

The FATC domains of all PIKKs are rather hydrophobic and rich in aromatic

residues (ATM & TOR see Fig. 1B). In line with this, all interact with membrane mimetics, although with somewhat different preferences for membrane features such as surface charge, curvature or packing density, and thus may all act as membrane anchoring units (32). Like TOR, ATM binds to all tested membrane mimetics including dodecylphosphocholine (DPC) micelles, bicelles composed of dimyristoyl and diheptanoylphosphocholine (DMPC, DihepPC), and small unilamellar vesicles (SUVs) made of DMPC (32). An estimate of the secondary structure content based on secondary chemical shifts suggested that the micelle-immersed human ATM FATC domain contains three helical stretches (32). Here, we present the determined NMR structure and an analysis of the relative orientation on the micelle and its membrane immersion properties and dynamics based on NMR and molecular dynamics (MD) data. We further prepared mutants by replacing conserved aromatic residues that are expected to be important for the membrane affinity and tested their ability to interact with DPC and DihepPC micelles, DMPC/DihepPC bicelles and DMPC SUVs. Overall the data provides a better understanding of the role of the AMT FATC domain in regulating the kinase function as well as the observed localization to specific membrane compartments.

Results

The NMR structure of micelle-immersed hATMfatc consists of three helices with a central flexible linker and a less flexible C-terminal linker

The three-dimensional structure of the human ATM FATC domain (hATMfatc) associated with DPC micelles (PDB-ID 6HKA) was determined by multidimensional heteronuclear NMR spectroscopy in solution. Since cleavage of the GB1tag is not efficient and results in very low yields, all structural restraints were derived from NMR data recorded for the GB1-tagged form (hATMfatc-gb1ent) (32). Previous studies have shown that the GB1tag does not affect the association with membrane mimetics and results only in little overlap of NMR signals of the GB1 tag and the FATC domain (41). The structural statistics are given in table 1.

The structure of micelle-associated hATMfatc, residues T68-V100 in hATMgatc-gb1ent corresponding to T3024-V3056 in full-length human ATM, consists of three helical regions (Fig. 1B-D). The structure is overall well-defined with 85.5% of the residues in the well structured region (V72-A83, P86-L92, P94-V100) occupying the most favored region of the Ramachandran plot (table 1). Based on the 20 lowest energy structures the N-terminal longer α-helix (α1) is on average formed by residues G73 to A83 of the 100 residues fusion protein, which corresponds to residues G3029 to 3039 of full-length human ATM. Following a three-residue linker (I84/3040-D85/3041-P86/3042), a second α-helix (α2) is on average formed by residues K87/3043-R91/3047. Following another proline-containing short linker (L92/3048-F93/3041-P94/3049), the C-terminal helix follows. Although tertiary contacts between the helices could not be observed, their orientation with respect to each other is not completely random. This may be explained by the presence of a proline in each linker. Based on the analysis of the conformations of short peptides based on residual dipolar couplings, prolines increase local order (42).

The central flexible linkage between α1 and α2 results in a high RMSD value of 4.47 Å for residues 70/3026-100/3056 compared to very low ones for the single helical regions (α1: 0.37 Å, α2: 0.22 Å, α3 0.27 Å, table 1) or the region including α2 and α3 (residues 87-99: 1.32 Å). This can be explained by the fact that no interhelical NOE contacts could be observed (table 1). In line with the dynamic linkage between α1 and α2 around D85/3041, it shows a $\{^{1}H\}$-^{15}N-NOE value of only 0.32 ± 0.10 at 150 mM and 298 K and 0.38 ± 0.11 at 200 mM and 298 K (Fig. 1D). The linkage between

α2 and α3 is also not rigid, but the {^{1}H}-^{15}N-NOE values in the linker region are not as low (L92/3048: 0.42, F93/3049: 0.48 at 150 mM DPC and 298 K) and of similar size as the ones for K97/3053 (0.43) and W99/3055 (0.48) in the short C-terminal helix. A more detailed description of the ^{15}N-relaxation data is provided in the SI (text and SI Fig. S1-S2).

Consistent with the differences in the amino acid sequence to the FATC domain of yeast TOR1 (= y1fatc, Fig. 1B top), the overall structural appearance is quite different. Y1fatc contains two conserved cysteines that can form a disulfide bond and oxidized y1fatc in the absence of membrane mimetics forms already an α-helix that is followed by a C-terminal disulfide bonded loop (43). In contrast, hATMfatc in buffer is largely unstructured and most backbone amide signals are not visible in the ^{1}H-^{15}N HSQC spectra (32), which hampers its resonance assignment.

Compared to micelle-associated hATMfatc, micelle-associated oxidized y1fatc adopts only a single α-helix that is followed a disulfide bonded loop or bulb (Fig. 1C right side) (44). Even in the reduced micelle-associated state of y1fatc the C-terminus folds back and the whole structure is less dynamic than that of hATMfatc (44). The {^{1}H}-^{15}N-NOE values of oxidized and reduced micelle-associated y1fatc at 298 K are more uniform in the well-structured region and do not show residues with significantly lower values in between (44) as observed for micelle associated hATMfatc (Fig. 1D).

The surface of micelle-associated hATMfatc (Fig. 2, top) is largely hydrophobic except for a positively charged surface region formed by K87/3043, R91/3047 and K97/3053 that is in neighborhood to a small negatively charged surface region formed by D85/3041. In contrast that of micelle-immersed y1fatc (Fig. 2 bottom) shows a large acidic region towards the N-terminus and only two small positively charged regions around K2448 and R2456. The C-terminal loop of y1fatc is largely hydrophobic (44).

The helical regions of micelle-associated hATMfatc can move with respect to each other

Additional insights into the dynamics as well as immersion properties (see next section) of micelle-associated hATMfatc were obtained from molecular dynamics simulations. In total 3 runs of MD simulations were performed using as starting structure for each one of the three lowest energy NMR structures (Fig. 3A). The simulation time for each run was 1.3 μs. The first 300 ns were discarded as equilibration time. As illustrated by the pictures of the simulated micelle-associated hATMfatc of each run (Fig. 3B), the relative orientation of the three helices with respect to each other various in each due to the dynamic linkages between the helices, especially the one between α1 and α2. Additional information about the conformational freedom are provided based on RMSD and RMSF (global and local) values in the SI (text and SI Fig. S4A-C). Consistent with the fact that no interhelical NOEs could be observed, distances below 0.5 nm between residues on different helices were only rarely and for very short simulation time periods observed (SI Fig. S4D). Plots of the angle between α1 and α2 as well as between α2 and α3 (Fig. 3C, SI Fig. S5A) as a function of time show that these angles can vary significantly as a function of the simulation time. Even with a simulation time of 1.3 ms, such simulations do usually not converge. In summary the ^{15}N-relaxation data and the MD simulations suggest that the reorientation of the helices with respect to each other due to the dynamic central linkage between α1 and α2 and less dynamic linkage between α2 and α3 is the major contribution to their dynamic properties, rather than more local conformational changes.

The hATM FATC domain resides largely in the head-group region of DPC micelles

Based on the MD simulations of the three lowest energy NMR structures of

micelle-associated hATMfatc in the presence of DPC micelles (Fig. 3), the three helices immerse mostly into the head-group region. To probe this experimentally, we recorded ^{1}H-^{15}N HSQC spectra of hATMfatc-gb1ent in the presence of DPC micelles (50 mM) and increasing amounts of paramagnetic 5- or 16-doxyl stearic acid (5-/16-SASL) (Fig. 4A, SI Fig. S5B). Earlier MD-simulations of DPC micellar systems in the absence and presence of protein showed that 5-/16-SASL can move in the micelle and that 16-SASL can bend such that the doxyl group is close to the head-group region and not deep in the interior as commonly assumed (45). The MD data further confirmed that the doxyl group of 5-SASL, as expected (46), resides also near the DPC head-groups (45). Residues of hATMfatc that localize close to the head-groups should thus show the strongest spectral changes. The doxyl label of 5- or 16-SASL results in paramagnetic relaxation enhancement (PRE), which reduces the signal intensity of nearby amide groups with an r^{-6} distance dependence (47). In order to better correlate the PRE effects with the average chemical shift changes (SI Fig. S6, S7) as well as with the distance from the micelle center of mass (COM, Fig. 4C, SI Fig. S8) and the surface area that is covered by DPC (Fig. 4D, SI Fig. S9) from the MD simulation, we plotted 1- I(x mM SASL)/I (0 mM SASL), which we refer to as 1-PRE. Thus, the stronger the PRE effect, the closer to 1 is the 1-PRE value (Fig. 4B, SI Fig. S6 and S7). As for the FATC domain of yeast TOR1, the PRE effects with 16-SASL are stronger than with 5-SASL (45). 1 mM 16-SASL results overall in somewhat larger 1-PRE values than 2 mM 5-SASL. Because the nitroxide spin-label usually does not induce significant pseudo contacts shifts, the observed chemical shift changes arise from a change in the chemical environment. Since the GB1 tag does not directly interact with the micelle, it shows only small 1-PRE values and average ^{1}H-^{15}N chemical shift changes (Fig. S6, S7). For the micelle-associating hATMfatc part the changes with 5- and 16-SASL show overall a similar trend as a function of the residue sequence position (Fig. 4A, B). Strong PRE effects (1-PRE $\geq$ 0.4) at 2 mM 5-SASL or 1 mM 16-SASL are seen for V72, I84, D85, F93, and G95. In case of 1 mM 16-SASL additionally for G73, L78, L79, Q81, Q82, A83, L92, K97, A98, and W99. Not surprisingly, many of them show also significant chemical shift changes (Fig. 4A, SI Fig. S6, S7). Since the listed residues based on the NMR data should localize near the head-groups they should have a distance from the micelle center of mass (COM) that is in a similar range as the phosphorus atom of the DPC head-group. Fig. 4C shows the average distance of the COM of each residue of hATMfatc to the micelle COM for run 1. Those for run 2 and 3 are displayed in SI Fig. S8. The profiles as a function of the sequence look very similar for all runs. In line with the 5- and 16-SASL NMR data, residues that show strong PRE effects (Fig. 4B) have mostly distances to the micelle COM that are similar to that of the DPC phosphorus atom (dotted line at 1.914 nm). In contrast, residues that show a small PRE effect, such as T68/3024 at the N-terminus of hATMfatc, show a larger distance to the micelle if they are more solvent accessible or a closer one such as for example L92/3046 if they reside deeper in the micelle. From a plot of the solvent accessible surface (SAS) area covered by DPC that was derived from the three MD runs (Fig. 4D, SI Fig. S9), it can further be estimated which residues immerse deeper and which should still be solvent accessible. As expected, those residues showing a short distance to the micelle COM (Fig. 3C, SI Fig. S8) are 80% or more covered by DPC, for e.g. run1 V72, V76, L79, P86, and L89. As expected, these residues are mostly hydrophobic.

In summary, the NMR data using spin-labeled micelles and the MD simulations of micelle-associated hATMfatc show that it binds the micelle by a dynamic assembly of three helices with many residues localizing in the head-group region.

None of the three helices penetrates the micelle very deeply or makes significant tertiary contacts to the other helices.

Mutation of F93/3049 and W96/3052 to alanine abrogates the association of hATMfatc with neutral SUVs but not with micelles and bicelles

Tryptophans but also other aromatic residues are known to play an important role for the affinity between membranes and proteins in general (48,49). For the FATC domain of TOR we have shown previously that replacement of up to 6 to 7 residues did not result in a significant abrogation of the association with micelles or bicelles. However, replacement of only one tyrosine (Y2463) or one tryptophan (W2466) resulted in an impairment of the interaction with SUVs (50). In order to find out if aromatic residues of hATMfatc at equivalent positions (F93/3049, W96/3052) have a similar effect, we mutated them individually and at the same time to alanine residues. The free states of the mutant proteins show even less peaks and thus appear to be more dynamic than wild type hATMfatc (SI Fig. S10, left side). This maybe explained with the smaller size of alanine compared to tyrosine or tryptophan. In the presence of 50 mM DPC, they adopt as the wild type a more ordered structure, which reduces the backbone dynamics such that the backbone and side chain amide signals become clearly visible (SI Fig. S10, right side). The interaction with neutral membrane mimetic micelles composed of DPC or the short chain diacyl lipid DihepPC, neutral bicelles composed of DMPC for the planar region and DihepPC for the rim, and small unilamellar vesicles composed of DMPC was further monitored by recording ^{1}H-^{15}N HSQC spectra in the absence and presence of these membrane mimetics (Fig. 5, SI Fig. S11, S12). As indicated by the observed spectral changes neither of these mutations abolished the interaction with micelles or bicelles (table 1). Whereas the single mutants F93/3049A and W96/3052A could still interact with neutral DMPC SUVs (SI Fig. S11, S12, green plus), a lack of spectral changes for the double mutant F93/3049A-W96/3052A (Fig. 4, lower right, red minus) indicates that it could not.

Discussion

ATM is not only involved in DNA repair but it has also been suggested that ATM plays a role in the oxidative stress response and as a link between genome stability and carbon metabolism (9,10). In line with this, it was recognized that ATM localizes not only in the nucleus but also at cytoplasmic vesicles (24) and more specifically peroxisomes (14) and microsomes (23), the plasma membrane (25), and mitochondria (15). NMR- and CD-monitored interaction studies showed that the ATM FATC domain can interact with all tested membrane mimetics, and thus may besides protein-protein interactions also mediate direct membrane interactions of ATM (32). The presented NMR structure of the micelle-associated state of the FATC domain of human ATM (Fig. 1, 2) and the characterization of its dynamic and immersion properties from MD and further NMR data (Fig. 3, 4) show that membrane association is mediated by three rather flexibly linked helices that immerse largely in the head-group region and slightly below and that do not significantly interact with each other. This dynamic assembly may enable specific interactions with other membrane embedded proteins. Recruitment to the plasma membrane involves interactions of the protein CKIP-1 (casein kinase-2 interaction protein-1) that is involved in muscle differentiation and the regulation of the actin cytoskeleton with the ATM C-terminal region, including the catalytic and the FATC domain (51). In addition, interactions with the PEX5 peroxisome import receptor localize ATM to peroxisomes (14).

The presence of a C-terminal positively charged surface patch next to a smaller negatively charged one in the micelle-associated ATM FATC domain (Fig. 2), may not only mediate interactions

with the positively and negatively charged head-group components of neutral phosphatidylcholines (PC) or phosphatidylethanolamines (PE) but additionally enable interactions with negatively charged phosphatidylserine (PS) in the PM or phosphorylated phosphosinositol lipids (PIPs) at mitochondria (52). The folding-upon-binding to a membrane mimetic, which has for example also been detected for the 30-residue long glucagon-like peptide 1 (GLP-1) (53), and the resulting dynamic helix assembly of membrane associated hATMfatc may further be helpful to interact with specific receptors or membranes with different packing densities, which depends e.g. on the amount of cholesterol or the ratio of saturated versus unsaturated fatty acids in the lipids (52). Based on the membrane catalysis hypothesis, initial interactions of signaling peptides with the bilayer increase their local concentration and allow them to adopt a structure that is recognized by the target membrane-resident receptors (53). The same maybe true for specific protein domains or segments.

Based on mutagenesis studies the FATC domains of all PIKKs play an important role for their regulation (26,30,31,33-35,54) and share the ability to interact with different membrane mimetics, albeit with varying preferences for specific membrane properties (32,44). The observed evolutionarily conserved sequence differences (e.g. Fig. 1B ATM and TOR) may result in different membrane associated conformations that determine the specific membrane targeting behavior (32). In line with this micelle-associated hATMfatc adopts a rather dynamic assembly of three helices with a hydrophobic N-terminal region and a more polar C-terminal one, whereas the one of the yeast TOR1 FATC domain consists of a single helix followed by a loop that in the oxidized state contains a disulfide bond and where the N-terminal region is acidic and the C-terminal one largely hydrophobic (Fig. 1C and Fig. 2). Consistent with this, the FATC domain of ATM cannot replace the one of ATR (29) or TOR (33).

The FATC domains of all PIKKs share conserved sequence features (e.g. Fig. 1B ATM and TOR) that maybe important for the regulatory function and especially for directly mediating membrane interactions (32). The conserved glycine near the C-terminus of TOR (G2465 of y1fatc (Fig. 1B), G2544 in human TOR) appears to facilitate the back bending of the C-terminal region to the α-helix (Fig. 1C, right side). Except for TRRAP, this glycine is also conserved in all other PIKKS (32) and in case of ATM participates in the flexible linkage between α2 and α3 (Fig. 1C center). The evolutionarily also completely conserved proline 3042 (= P86), aspartate 3041 (= D85), and alanine 3039 (= A83) of hATM form together with I3040 (= I84) in humans but a methionine in other organisms the flexible linker between α1 and α2. The proline and the aspartate are also found in the DNA-PKcs amino acid sequences from most organisms (humans D4113, P4114) and based on $^{13}C^{\alpha}$ secondary shifts also disrupt two helical stretches (32). Interestingly, alanine 3039 of hATMfatc is also in most other PIKKS conserved including TOR, in which the helix of the micelle-associated oxidized and reduced states is distorted around this residue (44).

All PIKK FATC domains contain at least one or more tryptophans and/or one or more tyrosine or phenylalanine and several aliphatic hydrophobic residues (32). Tryptophans are often found at the interface between the apolar interior and the polar aqueous environment (48,49) and many hydrophobic residues show a positive free energy contribution for the transfer of a model peptide from a lipid bilayer to water (55). Replacement of either Y2463 or W2466 (Y2542 and W2545 in human TOR) is already sufficient to abrogate the interaction of y1fatc with DMPC SUVs (50). For hATMfatc, F3049 (= F93) and W3052 (= W96) at equivalent positions have to be replaced simultaneously to achieve the same effect (Fig. 5, SI Fig. S11, S12). However,

the respective mutations did not abrogate the interaction with micelles and bicelles (Fig. 5, SI Fig. S10-S12). The different association behavior of FATC mutants with micelles and bicelles compared to SUVs can be explained twofold. First, in case of micelles or bicelles the total concentration of the used detergents or lipids and thus the available membrane mimetic surface area is much higher than for SUVs. The used concentration of DPC and DihepPC was 50 mM and the total lipid concentrations in the DMPC/DihepPC bicelle samples was ~240 mM. However due to the preparation method, the total lipid concentration in the SUV samples is significantly below 50 mM since pure DMPC cannot easily be resuspended at high concentrations and in addition some of the lipid is lost when separating the small from larger uni- and multilamellar vesicles by centrifugation. Whereas 1D ^{1}H NMR spectra can be used to compare the lipid content in samples with micelles and bicelles, this is due to the large size of SUVs and corresponding line broadening not possible. However, besides established methods such as dynamic light scattering, the CD signal can be used to compare different liposome preparations (50,56). A second reason for the different binding behavior of FATC domain to micelles and bicelles versus SUVs may further be a higher affinity for curved membrane surfaces. DPC micelles are rather small, spherical particles that contain ~50-60 DPC molecules, resulting in a molecular weight of ~19 kDa and a radius of gyration of about 17-18 Å (57,58). Bicelles have a rather planar bilayer region that is formed by a long chain phospholipid such as DMPC. However the rim that is formed by a short chain lipid such as DihepPC shows as micelles also a high curvature. The molecular weight of bicelles is usually >~250 kDa and the diameter of the planar region ranges from 21 to 77 Å for q values between 0.2 and 1 (59,60). Even liposomes of the SUV type are much larger than bicelles. Although they are as micelles approximately spherical, they are less curved since the radius is much larger (around 20-100 nm) (61). We suggested already earlier that for proteins with a rather high and broad affinity for different membrane mimetics, SUVs at the usually used lower concentrations are better suited to detect mutants that may also abrogate membrane association in localization studies in cells (50).

The characterization of the membrane association of ATM by NMR and MD simulations was done looking only at the FATC domain (Fig. 1-4). This raises the question how accessible it is for membrane-interactions in the context of the full-length protein. Based on recent cryo electron microscopy (EM) data, ATM was suggested to be in an equilibrium between a closed, inactive dimer (resolution ~4-6 Å) with restricted access to the substrate binding site and an open, active dimer (resolution ~11.5 Å, if combined data used 5.7 Å) with good access to the substrate binding side (40). Whereas the FATC domain appears not well accessible in the closed, inactive ATM dimer, it appears well accessible for interactions with membranes and regulatory proteins in the open, active state. The conformation of the FATC domain in the provided cryo EM structures is similar to the micelle-associated conformation presented here and also consists to two α-helices and a C-terminal helix or turn-like structure (40). Early studies suggested that DNA damages induce Ser1981 autophosphorylation and that this results in active, monomeric ATM (62), in which the FATC domain is expected to be even better accessible than in the open dimer. Moreover, studies of oxidative activation of ATM indicated that oxidation of Cys2991 which is about 60-80 residues N-terminal of the FATC domain, results in dimerization (63). Thus future membrane-interactions studies may analyze the effect of reactive oxygen species (ROS) or oxidized lipids on C2991. Future localization studies of ATM in cells have to clarify how it varies in response to specific signals and which interactions with specific,

especially membrane localized proteins such as the PEX5 peroxisome import receptor (14), as well as membrane regions and specific signaling lipids it involves. Moreover, the oligomerization state under different signaling conditions and the resulting cellular localizations have to be determined. Finally, acetylation of lysine 3016 (54) N-terminal of the highly conserved FATC region of ATM may effect the described localization at the plasma membrane, mitochondria, peroxisomes, mircrosomes, and other cytosolic vesicles (12,14,15,23-25).

As suggested for the FATC domain of TOR, the one of ATM may also be fused to other proteins or peptides or other substances to tether them to membrane mimetics (64).

Experimental Procedures

Plasmid cloning, protein expression, and purification

The coding sequence for the FAT C-terminal (FATC) domain of human ATM (residues 3024-3056, UniProt-ID 13315) was cloned into GEV2 (65). The resulting fusion protein consisting of GB1 (residues 1-56), a linker region composed of a thrombin (57-62) and an enterokinase (63-67) protease recognition site, and the C-terminal 33 residue of human ATM (68-100) (= hATMfatc-gb1ent) was overexpressed in *Escherichia coli* BL21 at 37 ºC. Since proteolytic removal of the GB1tag is inefficient and the GB1 tag does not disturb the interaction with membrane mimetics and its monitoring, the fusion protein was used for the described NMR studies (32,41). Uniformly ^{15}N-, or ^{15}N-^{13}C –labeled proteins were prepared in M9 minimal medium containing $^{15}NH_4Cl$ and/or ^{13}C-glucose as the sole nitrogen and carbon sources. The expression and the purification by a heating step (66) and IgG affinity chromatography were done as described previously (32,67).

Site-directed mutagenesis

Replacement of one or more aromatic residue in hATMfatc-gb1ent by alanine (Fig. 1B, F93A = F3049A, W96A = W3052A, F93A/W96A = F3049A/W3052A) was achieved by following the QuickChange site-directed mutagenesis protocol (Stratagene). The success of the mutagenesis was verified by DNA sequencing. Cells expressing mutant hATMfatc-gb1ent were lysed by sonication in 50 mM Tris, 150 mM NaCl, 2 mM benzamidine and 0.3 mM EDTA, pH 7.6. Mutant proteins were purified by IgG affinity chromatography as described for the wild type and in the manufacturer's manual (32,67). Fractions containing the target protein were pooled, washed with NMR buffer (50 mM Tris, 100 mM NaCl, pH 7.4 for the single mutants F93A = F3049A, W96A = W3052A or pH 6.5 for the double mutant F93A/W96A = F3049A/W3052A), and concentrated.

Preparation of membrane-mimetics

Dodecylphosphocholine (DPC), 1,2-diheptanoyl-*sn*-glycero-3-phosphocholine (DihepPC), 1,2-dimyristoyl-*sn*-glycero-3-phosphocholine (DMPC), 5-doxyl stearic acid (5-SASL), and 16-doxyl stearic acid (16-SASL) were purchased from Avanti Polar Lipids and/or Sigma-Aldrich. Deuterated DPC (d_{38}-DPC) was obtained from Cambridge Isotopes.

Membrane mimetic DPC micelles were prepared by placing a defined amount of DPC from concentrated stock solution in chloroform (0.5 M) in a glass vial and drying under a stream of nitrogen gas. The resulting DPC film was dissolved in NMR buffer containing the protein of interest. For NMR titration experiments samples containing >30 mM DPC were prepared in the same way, whereas those with DPC concentrations < 30 mM were prepared by diluting a 100 mM DPC stock in buffer with a protein stock and buffer. Note that a separate sample was prepared for each DPC concentration to avoid dilution effects and thus to keep the protein concentration

constant. DihepPC micelles were prepared by diluting a 0.25 M stock solution in NMR buffer to 50 mM with the respective protein solution and buffer. Micelles form above the critical micelle concentration (CMC), which is 1.1 mM for DPC (68) and 1.4-1.8 mM for DihepPC (69,70).

DMPC/DihepPC bicelles (q= 0.2, [DMPC] = 0.04 M, and [DihepPC] = 0.20 M, cL 15%) were prepared as follows. An appropriate amount of a 0.25 M stock of the long-chain phospholipid (DMPC) in chloroform was placed in a glass vial and the chloroform blown away under a stream of nitrogen gas. In order to form bicelles, the right amount of the short-chain lipid (DihepPC) in NMR buffer was added and the vial vortexed until a clear solution was obtained. Lastly, the protein solution was added to the concentrated bicelles solution.

Liposomes were prepared by drying an appropriate amount of DMPC in chloroform (0.25 M) under a stream of nitrogen gas. The resulting pellet was dissolved in NMR buffer to obtain a 100 mM solution. To dissolve the pellet, it was exposed to seven cycles of freezing in liquid nitrogen, thawing by incubation in a water bath at 40 °C and thorough vortexing. To induce the formation of small unilamellar vesicles (SUVs) from large uni- and multilamellar vesicles, the DMPC suspension was incubated in an ultra-sonication bath for 30 minutes. A clear supernatant containing only SUVs was obtained after centrifuging the lipid mixture at about 15 krpm in a table top centrifuge for 5 minutes. The resulting white precipitate at the bottom corresponds to large uni- and multilamellar vesicles. For the preparation of a protein sample in the presence of liposomes, only the clear supernatant containing small unilamellar vesicles was diluted 1:1 with protein solution. Thus, using the 100 mM stock solution the final sample contained < 50 mM DMPC.

NMR sample preparation

For the NMR resonance assignment and structural characterization samples containing ~0.5 mM of ^{15}N or ^{15}N-^{13}C-hATMfatc-gb1ent in 50 mM Tris, 100 mM NaCl, 10 mM TCEP, 0.02% NaN_3 (95% H_2O/5% D_2O), pH 6.5, 150 mM d_{38}-DPC were used. We also prepared samples with 200 mM d_{38}-DPC (180 mM d38-DPC and 20 mM DPC), but the spectral quality was overall lower (broader signals, more noise signals) than for samples with 150 mM DPC (see e.g. SI Fig. S1). The 10% ^{13}C-labeled hATMfatc-gb1ent sample used for the stereospecific assignment of valine and leucine methyl groups contained 170 mM d_{38}-DPC micelles.

The samples of hATMfatc-gb1ent mutants contained about 0.15 mM ^{15}N-labeled protein in NMR buffer. For the double mutant (F93/W96 = F3049A/W3052A) the pH was 6.5, as for the wild type. The single mutants (F93 = F3049A, W96 = W3052A) were measured at pH 7.4 to improve their solubility and stability.

For NMR experiments with spin-labeled DPC micelles, samples containing about 0.1 mM protein and 50 mM undeuterated DPC were prepared. The concentration of 5- and 16-doxyl stearic acid (5-/16-SASL) was increased by stepwise addition of a small amount (1 to at maximum 4 mM) from a 0.25 M stock solution in chloroform.

NMR spectroscopy

NMR spectra were recorded on Bruker Avance 500 MHz, 600 MHz, and 900 MHz spectrometers at a temperature of 298 K. The 500 MHz and 900 MHz spectrometer were equipped with cryogenic probes. Data were processed with NMRPipe (71) and analyzed using NMRView (72). Assignments for the ^{13}C, ^{15}N, and ^{1}H nuclei of micelle-immersed hATMfatc fusion protein were based on 2D ^{1}H-^{15}N and various ^{1}H-^{13}C HSQC spectra, partially without decoupling, 3D HNCA, HNCACB, CCONH-TOCSY, HCCH-TOCSY, HNHA, HNHB and ^{15}N- and ^{13}C-edited NOESY spectra as described (67). The NOESY mixing times were 90 ms for the ^{15}N-edited

NOESY, 100 ms for the aromatic and aliphatic ^{13}C-edited NOESY experiments. Information about backbone dynamics was derived from the analysis of ^{15}N relaxation data, including T_1 (spin-lattice longitudinal relaxation rate), T_2 (spin-spin or transverse relaxation rate), and $\{^1H\}$-^{15}N NOE.

The immersion depth properties of hATMfatc in DPC micelles were derived by recording ^{1}H-^{15}N HSQC and 1D ^{1}H-NMR spectra of samples containing increasing amounts of paramagnetic 5- or 16-doxyl stearic acid (5- and 16-SASL). The resulting paramagnetic relaxation enhancement (PRE) effects were derived based on the observed changes in signal intensity. Since the spectral changes with 5-SASL were overall smaller compared to 16-SASL, 1-PRE values for 2 mM were analyzed for 5-SASL and for 1 mM for 16-SASL. In addition, the average chemical shift changes of the backbone amide nitrogen and proton $[\Delta\delta(N,H)_{av}]$ were calculated based on the formula $[(\Delta\delta_{HN})^2 + (\Delta\delta_N/5)^2]^{1/2}$. The interaction of mutant proteins with membrane mimetics was monitored by recording 1D ^{1}H and 2D ^{1}H-^{15}N HSQC spectra.

Structure calculation

All structure calculations were performed with XPLOR-NIH (73) using molecular dynamics in torsion angle and Cartesian coordinate space and the standard force field with the parameter files topallhdg_new.pro and parallhdg_new.pro. Distance restraints were generated in NMRView (72) and classified according to NOE-cross peak intensities. Upper bounds were 2.8 Å, 3.5 Å, 4.5 Å and 5.5 Å. The lower bound was always 1.8 Å. For all NOE restraints r^{-6} sum averaging was used. Backbone dihedral angle restraints for ϕ and ψ as well as hydrogen bond restraints for helical regions were derived based on the determined $^{13}C^{\alpha}$ chemical shifts, observed helix typical NOE restraints and on initial structure calculations.

MD simulations

Molecular dynamics simulations were performed with Gromacs 2016.3 software (74-76). The FATC domain was initially placed randomly near the preequilibrated micelle (50 DPC molecules) and solvated with ~54000 water molecules (box size ~11 nm). Na^+ and Cl^- ions were added to the system to reach 0.1 M salt concentration. The CHARMM36m force field was used for the protein and DPC (77). A 2 fs time step was used. All bonds were constrained with the LINCS algorithm (78) and water bond lengths and angles were kept constant using the SETTLE algorithm (79). Initial velocities were taken from the Maxwell distribution for 303.15 K. A constant temperature of 303.15 K was maintained with the V-rescale thermostat with 0.1 ps coupling constant (80). The DPC micelle with the protein and the water molecules with the ions were coupled to two separate thermostats with the same parameters. Constant pressure of 1 bar was maintained by the isotropic Parrinello-Rahman barostat with 5.0 ps coupling constant and $4.5*10^{-5}$ bar^{-1} compressibility (81). The particle mesh Ewald (PME) algorithm was used for long-range contributions to electrostatic interactions (82,83). Lennard-Jones interactions were cut off at 1.2 nm with a force-switch modifier from 1.0 to 1.2 nm.

Three independent simulations were performed using as starting structures the three lowest energy NMR structures of the micelle-associated FATC domain of human ATM. Each simulation was 1.3 microseconds long. For the analysis of the secondary structure based on DSSP calculations (84), the clustering, the immersion depth, and the fraction of solvent accessible surface area covered by the micelle, the first 300 ns of each simulation were discarded as equilibration time.

RMSD and RMSF calculations were performed on the last 500 ns of each trajectory (800-1300 ns). RMSF analysis with the local fit of the protein structure was

performed in addition to the calculations with a whole protein as a reference. The RMSD/RMSF is dominated by the contributions from a change in relative orientation of the helices and we wanted to highlight local fluctuations in particular regions which aren't the result of the change in helix-helix orientation. RMSF graphs that are marked as 'local 72-92' or 'local 86-98' (SI Fig. S4) were calculated with the use of a short part of the protein as a reference for the progressive trajectory fitting and subsequent RMSF calculation (residues 72-92, 86-98; 5 ns windows with the following averaging over all 5 ns intervals). Consequently, the RMSF values will be rather small for the region used for the fit.

The analysis of the angles between the helices in Fig. 3C (SI Fig. S5) starts also from 800 ns, because the relative orientation of the helices changes slowly compared to the local structure of the protein. Thus we let the system equilibrate for a longer period of time to have less bias from the initial structure.

The distance between the micelle center of mass (COM) and the whole peptide COM, as well as separate peptide residue COMs, was computed using the simulation period from 300-1300 ns. To analyze peptide stability, the secondary structure of each peptide was computed as a function of time with the gmx do_dssp analysis program, which is part of the Gromacs package. The micelle surface for the images of the micelle associated FATC domain was defined as an iso-surface of averaged DPC density (contour density of 0.250 atoms/A^3). The pictures of the FATC domain alone are representative conformations of the protein as defined by cluster analysis of the protein RMSD performed by the gmx cluster program with the GROMOS clustering algorithm and 0.1 nm cutoff. All three trajectories (excluding the first 300 ns of each run) were combined into a single set of structures and cluster analysis was performed on this combined trajectory. Subsequently, 10 structures, one from each of the first 10 most populated clusters were selected as representative structures of the micelle-associated ATM FATC domain. The central structures of each cluster (in terms of RMSD distance) were selected as a representative for a given cluster. The combined size of the 10 most populated clusters was equal to 69.3% of the complete set of structures sampled. For the picture of a selective structure of micelle-associated hATMfatc for each run, a clustering analysis for reach run was performed. From the most populated cluster a structure with an RMSD corresponding to the average for the whole cluster, thus being in the middle, was selected. To estimate if there are interhelical contacts below about 0.5 nm that could give rise to NOEs, interresidue distances were calculated between the centers of mass for pairs of residues that belong to different helices (excluding adjacent residue pairs, SI Fig. S4D).

Acknowledgements: We thank Martin Schaad, Lisa A. M. Sommer and Anja Wacker for their previous contributions to the project.

Conflict of interest: The authors declare that they have no conflicts of interest with the contents of this article.

Author contributions: SAD designed the study. MSAR performed the NMR experiments, analyzed the results and calculated the structures supported by SAD. DPT and YKC designed the MD simulations and YKC performed the simulations and analyzed the corresponding results. SAD wrote the paper with MSAR, YKC, and DPT.

References

1. Lovejoy, C. A., and Cortez, D. (2009) Common mechanisms of PIKK regulation. *DNA repair* **8**, 1004-1008
2. Abraham, R. T. (2001) Cell cycle checkpoint signaling through the ATM and ATR kinases. *Genes & development* **15**, 2177-2196
3. Chen, B. P., Li, M., and Asaithamby, A. (2012) New insights into the roles of ATM and DNA-PKcs in the cellular response to oxidative stress. *Cancer letters* **327**, 103-110
4. Lempiainen, H., and Halazonetis, T. D. (2009) Emerging common themes in regulation of PIKKs and PI3Ks. *The EMBO journal* **28**, 3067-3073
5. Quek, H., Lim, Y. C., Lavin, M. F., and Roberts, T. L. (2018) PIKKing a way to regulate inflammation. *Immunology and cell biology* **96**, 8-20
6. Pancholi, N. J., Price, A. M., and Weitzman, M. D. (2017) Take your PIKK: tumour viruses and DNA damage response pathways. *Philosophical transactions of the Royal Society of London. Series B, Biological sciences* **372**
7. Gonzalez, A., and Hall, M. N. (2017) Nutrient sensing and TOR signaling in yeast and mammals. *The EMBO journal* **36**, 397-408
8. Ma, Y., Vassetzky, Y., and Dokudovskaya, S. (2018) mTORC1 pathway in DNA damage response. *Biochimica et biophysica acta* **1865**, 1293-1311
9. Ditch, S., and Paull, T. T. (2012) The ATM protein kinase and cellular redox signaling: beyond the DNA damage response. *Trends in biochemical sciences* **37**, 15-22
10. Kruger, A., and Ralser, M. (2011) ATM is a redox sensor linking genome stability and carbon metabolism. *Science signaling* **4**, pe17
11. Cam, H., Easton, J. B., High, A., and Houghton, P. J. (2010) mTORC1 signaling under hypoxic conditions is controlled by ATM-dependent phosphorylation of HIF-1alpha. *Molecular cell* **40**, 509-520
12. Alexander, A., Cai, S. L., Kim, J., Nanez, A., Sahin, M., MacLean, K. H., Inoki, K., Guan, K. L., Shen, J., Person, M. D., Kusewitt, D., Mills, G. B., Kastan, M. B., and Walker, C. L. (2010) ATM signals to TSC2 in the cytoplasm to regulate mTORC1 in response to ROS. *Proceedings of the National Academy of Sciences of the United States of America* **107**, 4153-4158
13. Shen, C., and Houghton, P. J. (2013) The mTOR pathway negatively controls ATM by up-regulating miRNAs. *Proceedings of the National Academy of Sciences of the United States of America* **110**, 11869-11874
14. Zhang, J., Tripathi, D. N., Jing, J., Alexander, A., Kim, J., Powell, R. T., Dere, R., Tait-Mulder, J., Lee, J. H., Paull, T. T., Pandita, R. K., Charaka, V. K., Pandita, T. K., Kastan, M. B., and Walker, C. L. (2015) ATM functions at the peroxisome to induce pexophagy in response to ROS. *Nature cell biology* **17**, 1259-1269
15. Valentin-Vega, Y. A., Maclean, K. H., Tait-Mulder, J., Milasta, S., Steeves, M., Dorsey, F. C., Cleveland, J. L., Green, D. R., and Kastan, M. B. (2012) Mitochondrial dysfunction in ataxia-telangiectasia. *Blood* **119**, 1490-1500
16. Paull, T. T. (2015) Mechanisms of ATM Activation. *Annual review of biochemistry*
17. Marinoglou, K. (2012) The role of the DNA damage response kinase ataxia telangiectasia mutated in neuroprotection. *The Yale journal of biology and medicine* **85**, 469-480
18. Cremona, C. A., and Behrens, A. (2014) ATM signalling and cancer. *Oncogene* **33**, 3351-3360

19. Mugler, A., Tostevin, F., and Ten Wolde, P. R. (2013) Spatial partitioning improves the reliability of biochemical signaling. *Proceedings of the National Academy of Sciences of the United States of America*
20. Czarny, P., Pawlowska, E., Bialkowska-Warzecha, J., Kaarniranta, K., and Blasiak, J. (2015) Autophagy in DNA damage response. *International journal of molecular sciences* **16**, 2641-2662
21. Shiloh, Y., and Ziv, Y. (2013) The ATM protein kinase: regulating the cellular response to genotoxic stress, and more. *Nat Rev Mol Cell Biol* **14**, 197-210
22. De Cicco, M., Abd Rahim, M. S., and Dames, S. A. (2015) Regulation of the Target of Rapamycin and Other Phosphatidylinositol 3-Kinase-Related Kinases by Membrane Targeting. *Membranes* **5**, 553-575
23. Brown, K. D., Ziv, Y., Sadanandan, S. N., Chessa, L., Collins, F. S., Shiloh, Y., and Tagle, D. A. (1997) The ataxia-telangiectasia gene product, a constitutively expressed nuclear protein that is not up-regulated following genome damage. *Proceedings of the National Academy of Sciences of the United States of America* **94**, 1840-1845
24. Watters, D., Khanna, K. K., Beamish, H., Birrell, G., Spring, K., Kedar, P., Gatei, M., Stenzel, D., Hobson, K., Kozlov, S., Zhang, N., Farrell, A., Ramsay, J., Gatti, R., and Lavin, M. (1997) Cellular localisation of the ataxia-telangiectasia (ATM) gene product and discrimination between mutated and normal forms. *Oncogene* **14**, 1911-1921
25. Yan, J., Khanna, K. K., and Lavin, M. F. (2000) Defective radiation signal transduction in ataxia-telangiectasia cells. *International journal of radiation biology* **76**, 1025-1035
26. Bosotti, R., Isacchi, A., and Sonnhammer, E. L. (2000) FAT: a novel domain in PIK-related kinases. *Trends in biochemical sciences* **25**, 225-227
27. Perry, J., and Kleckner, N. (2003) The ATRs, ATMs, and TORs are giant HEAT repeat proteins. *Cell* **112**, 151-155
28. Knutson, B. A. (2010) Insights into the domain and repeat architecture of target of rapamycin. *Journal of structural biology* **170**, 354-363
29. Mordes, D. A., Glick, G. G., Zhao, R., and Cortez, D. (2008) TopBP1 activates ATR through ATRIP and a PIKK regulatory domain. *Genes & development* **22**, 1478-1489
30. Keith, C. T., and Schreiber, S. L. (1995) PIK-related kinases: DNA repair, recombination, and cell cycle checkpoints. *Science* **270**, 50-51
31. Jiang, X., Sun, Y., Chen, S., Roy, K., and Price, B. D. (2006) The FATC domains of PIKK proteins are functionally equivalent and participate in the Tip60-dependent activation of DNA-PKcs and ATM. *The Journal of biological chemistry* **281**, 15741-15746
32. Sommer, L. A. M., Schaad, M., and Dames, S. A. (2013) NMR- and Circular Dichroism-monitored Lipid Binding Studies Suggest a General Role for the FATC Domain as Membrane Anchor of Phosphatidylinositol 3-Kinase-related Kinases (PIKK). *Journal of Biological Chemistry* **288**, 20046-20063
33. Takahashi, T., Hara, K., Inoue, H., Kawa, Y., Tokunaga, C., Hidayat, S., Yoshino, K., Kuroda, Y., and Yonezawa, K. (2000) Carboxyl-terminal region conserved among phosphoinositide-kinase-related kinases is indispensable for mTOR function in vivo and in vitro. *Genes to cells : devoted to molecular & cellular mechanisms* **5**, 765-775
34. Hoke, S. M., Irina Mutiu, A., Genereaux, J., Kvas, S., Buck, M., Yu, M., Gloor, G. B., and Brandl, C. J. (2010) Mutational analysis of the C-terminal FATC domain of Saccharomyces cerevisiae Tra1. *Current genetics* **56**, 447-465

35. Morita, T., Yamashita, A., Kashima, I., Ogata, K., Ishiura, S., and Ohno, S. (2007) Distant N- and C-terminal domains are required for intrinsic kinase activity of SMG-1, a critical component of nonsense-mediated mRNA decay. *The Journal of biological chemistry* **282**, 7799-7808
36. Llorca, O., Rivera-Calzada, A., Grantham, J., and Willison, K. R. (2003) Electron microscopy and 3D reconstructions reveal that human ATM kinase uses an arm-like domain to clamp around double-stranded DNA. *Oncogene* **22**, 3867-3874
37. Lau, W. C., Li, Y., Liu, Z., Gao, Y., Zhang, Q., and Huen, M. S. (2016) Structure of the human dimeric ATM kinase. *Cell cycle* **15**, 1117-1124
38. Sawicka, M., Wanrooij, P. H., Darbari, V. C., Tannous, E., Hailemariam, S., Bose, D., Makarova, A. V., Burgers, P. M., and Zhang, X. (2016) The Dimeric Architecture of Checkpoint Kinases Mec1ATR and Tel1ATM Reveal a Common Structural Organization. *The Journal of biological chemistry* **291**, 13436-13447
39. Wang, X., Chu, H., Lv, M., Zhang, Z., Qiu, S., Liu, H., Shen, X., Wang, W., and Cai, G. (2016) Structure of the intact ATM/Tel1 kinase. *Nature communications* **7**, 11655
40. Baretic, D., Pollard, H. K., Fisher, D. I., Johnson, C. M., Santhanam, B., Truman, C. M., Kouba, T., Fersht, A. R., Phillips, C., and Williams, R. L. (2017) Structures of closed and open conformations of dimeric human ATM. *Science advances* **3**, e1700933
41. Sommer, L. A. M., Meier, M. A., and Dames, S. A. (2012) A fast and simple method for probing the interaction of peptides and proteins with lipids and membrane-mimetics using GB1 fusion proteins and NMR spectroscopy. *Protein science : a publication of the Protein Society* **21**, 1566-1570
42. Dames, S. A., Aregger, R., Vajpai, N., Bernado, P., Blackledge, M., and Grzesiek, S. (2006) Residual dipolar couplings in short peptides reveal systematic conformational preferences of individual amino acids. *Journal of the American Chemical Society* **128**, 13508-13514
43. Dames, S. A., Mulet, J. M., Rathgeb-Szabo, K., Hall, M. N., and Grzesiek, S. (2005) The solution structure of the FATC domain of the protein kinase target of rapamycin suggests a role for redox-dependent structural and cellular stability. *The Journal of biological chemistry* **280**, 20558-20564
44. Dames, S. A. (2010) Structural basis for the association of the redox-sensitive target of rapamycin FATC domain with membrane-mimetic micelles. *The Journal of biological chemistry* **285**, 7766-7775
45. Sommer, L. A. M., Janke, J. J., Bennett, W. F. D., Bürck, J., Ulrich, A. S., Tieleman, D. P., and Dames, S. A. (2014) Characterization of the Immersion Properties of the Peripheral Membrane Anchor of the FATC Domain of the Kinase "Target of Rapamycin" by NMR, Oriented CD Spectroscopy, and MD Simulations. *The Journal of Physical Chemistry B* **118**, 4817-4831
46. Koehler, J., and Meiler, J. (2011) Expanding the utility of NMR restraints with paramagnetic compounds: background and practical aspects. *Prog Nucl Magn Reson Spectrosc* **59**, 360-389
47. Yagi, H., Loscha, K. V., Su, X. C., Stanton-Cook, M., Huber, T., and Otting, G. (2010) Tunable paramagnetic relaxation enhancements by [Gd(DPA)(3)] (3-) for protein structure analysis. *Journal of biomolecular NMR* **47**, 143-153
48. Sun, H., Greathouse, D. V., Andersen, O. S., and Koeppe, R. E., 2nd. (2008) The preference of tryptophan for membrane interfaces: insights from N-methylation of tryptophans in gramicidin channels. *The Journal of biological chemistry* **283**, 22233-22243

49. Liu, W., and Caffrey, M. (2006) Interactions of tryptophan, tryptophan peptides, and tryptophan alkyl esters at curved membrane interfaces. *Biochemistry* **45**, 11713-11726
50. Sommer, L. A. M., and Dames, S. A. (2014) Characterization of residue-dependent differences in the peripheral membrane association of the FATC domain of the kinase 'target of rapamycin' by NMR and CD spectroscopy. *FEBS letters* **588**, 1755-1766
51. Zhang, L., Tie, Y., Tian, C., Xing, G., Song, Y., Zhu, Y., Sun, Z., and He, F. (2006) CKIP-1 recruits nuclear ATM partially to the plasma membrane through interaction with ATM. *Cellular signalling* **18**, 1386-1395
52. Sprong, H., van der Sluijs, P., and van Meer, G. (2001) How proteins move lipids and lipids move proteins. *Nat Rev Mol Cell Biol* **2**, 504-513
53. Myers, G. A., Gacek, D. A., Peterson, E. M., Fox, C. B., and Harris, J. M. (2012) Microscopic rates of Peptide-phospholipid bilayer interactions from single-molecule residence times. *Journal of the American Chemical Society* **134**, 19652-19660
54. Sun, Y., Jiang, X., Chen, S., Fernandes, N., and Price, B. D. (2005) A role for the Tip60 histone acetyltransferase in the acetylation and activation of ATM. *Proceedings of the National Academy of Sciences of the United States of America* **102**, 13182-13187
55. Wimley, W. C., and White, S. H. (1996) Experimentally determined hydrophobicity scale for proteins at membrane interfaces. *Nat Struct Biol* **3**, 842-848
56. Rodriguez Camargo, D. C., Link, N. M., and Dames, S. A. (2012) The FKBP-rapamycin binding domain of human TOR undergoes strong conformational changes in the presence of membrane mimetics with and without the regulator phosphatidic acid. *Biochemistry* **51**, 4909-4921
57. Lazaridis, T., Mallik, B., and Chen, Y. (2005) Implicit solvent simulations of DPC micelle formation. *The journal of physical chemistry. B* **109**, 15098-15106
58. Tieleman, D. P. v. d. S., D.; Berendsen, H.J.C. (2000) Molecular Dynamics Simulations of Dodecylphosphocholine Micelles at Three Different Aggregate Sizes: Micellar Structure and Chain Relaxation. *J. Phys. Chem. B* **104**, 6380-6388
59. Whiles, J. A., Deems, R., Vold, R. R., and Dennis, E. A. (2002) Bicelles in structure-function studies of membrane-associated proteins. *Bioorganic chemistry* **30**, 431-442
60. Luchette, P. A., Vetman, T. N., Prosser, R. S., Hancock, R. E., Nieh, M. P., Glinka, C. J., Krueger, S., and Katsaras, J. (2001) Morphology of fast-tumbling bicelles: a small angle neutron scattering and NMR study. *Biochimica et biophysica acta* **1513**, 83-94
61. Lin, C. M., Li, C. S., Sheng, Y. J., Wu, D. T., and Tsao, H. K. (2012) Size-dependent properties of small unilamellar vesicles formed by model lipids. *Langmuir : the ACS journal of surfaces and colloids* **28**, 689-700
62. Bakkenist, C. J., and Kastan, M. B. (2003) DNA damage activates ATM through intermolecular autophosphorylation and dimer dissociation. *Nature* **421**, 499-506
63. Guo, Z., Kozlov, S., Lavin, M. F., Person, M. D., and Paull, T. T. (2010) ATM activation by oxidative stress. *Science* **330**, 517-521
64. De Cicco, M., Milroy, L. G., and Dames, S. A. (2018) Target of rapamycin FATC domain as a general membrane anchor: The FKBP-12 like domain of FKBP38 as a case study. *Protein science : a publication of the Protein Society* **27**, 546-560
65. Huth, J. R., Bewley, C. A., Jackson, B. M., Hinnebusch, A. G., Clore, G. M., and Gronenborn, A. M. (1997) Design of an expression system for detecting folded protein domains and mapping macromolecular interactions by NMR. *Protein science : a publication of the Protein Society* **6**, 2359-2364

66. Koenig, B. W., Rogowski, M., and Louis, J. M. (2003) A rapid method to attain isotope labeled small soluble peptides for NMR studies. *Journal of biomolecular NMR* **26**, 193-202
67. Abd Rahim, M. S., Sommer, L. A. M., Wacker, A., Schaad, M., and Dames, S. A. (2018) 1H, 15N, and 13C chemical shift assignments of the micelle immersed FAT C-terminal (FATC) domains of the human protein kinases ataxia-telangiectasia mutated (ATM) and DNA-dependent protein kinase catalytic subunit (DNA-PKcs) fused to the B1 domain of streptococcal protein G (GB1). *Biomolecular NMR assignments*
68. Stafford, R. E., Fanni, T., and Dennis, E. A. (1989) Interfacial properties and critical micelle concentration of lysophospholipids. *Biochemistry* **28**, 5113-5120
69. Tausk, R. J., Karmiggelt, J., Oudshoorn, C., and Overbeek, J. T. (1974) Physical chemical studies of short-chain lecithin homologues. I. Influence of the chain length of the fatty acid ester and of electrolytes on the critical micelle concentration. *Biophysical chemistry* **1**, 175-183
70. Weschayanwiwat, P., Scamehorn, J., and Reilly, P. (2005) Surfactant properties of low molecular weight phospholipids. *Journal of Surfactants and Detergents* **8**, 65-72
71. Delaglio, F., Grzesiek, S., Vuister, G. W., Zhu, G., Pfeifer, J., and Bax, A. (1995) NMRPipe: a multidimensional spectral processing system based on UNIX pipes. *Journal of biomolecular NMR* **6**, 277-293
72. Johnson, B. A. (2004) Using NMRView to visualize and analyze the NMR spectra of macromolecules. *Methods in molecular biology* **278**, 313-352
73. Schwieters, C. D., Kuszewski, J. J., Tjandra, N., and Clore, G. M. (2003) The Xplor-NIH NMR molecular structure determination package. *Journal of magnetic resonance* **160**, 65-73
74. Van Der Spoel, D., Lindahl, E., Hess, B., Groenhof, G., Mark, A. E., and Berendsen, H. J. (2005) GROMACS: fast, flexible, and free. *Journal of computational chemistry* **26**, 1701-1718
75. Hess, B., Kutzner, C., van der Spoel, D., and Lindahl, E. (2008) GROMACS 4: Algorithms for Highly Efficient, Load-Balanced, and Scalable Molecular Simulation. *J. Chem. Theory Comput.* **4**, 435-447
76. Abraham, M. J., Murtola, T., Schulz, R., Páll, S., Smith, J. C., Hess, B., and Lindahl, E. (2015) GROMACS: High performance molecular simulations through multi-level parallelism from laptops to supercomputers. *SoftwareX* **1-2**, 19-25
77. Huang, J., Rauscher, S., Nawrocki, G., Ran, T., Feig, M., de Groot, B. L., Grubmuller, H., and MacKerell, A. D., Jr. (2017) CHARMM36m: an improved force field for folded and intrinsically disordered proteins. *Nature methods* **14**, 71-73
78. Hess, B., Bekker, H., Berendsen, H. J. C., and Fraaije, J. G. E. M. (1997) LINCS: A linear constraint solver for molecular simulations. *Journal of computational chemistry* **18**, 1463-1472
79. Miyamoto, S., and Kollman, P. A. (1992) Settle - an Analytical Version of the Shake and Rattle Algorithm for Rigid Water Models. *Journal of computational chemistry* **13**, 952-962
80. Bussi, G., Donadio, D., and Parrinello, M. (2007) Canonical sampling through velocity rescaling. *The Journal of chemical physics* **126**, 014101
81. Parrinello, M., and Rahman, A. (1981) Polymorphic transitions in single crystals: A new molecular dynamics method. *Journal of Applied Physics* **52**, 7182-7190

82. Darden, T., York, D., and Pedersen, L. (1993) Particle Mesh Ewald - an N.Log(N) Method for Ewald Sums in Large Systems. *Journal of Chemical Physics* **98**, 10089-10092
83. Essmann, U., Perera, L., Berkowitz, M. L., Darden, T., Lee, H., and Pedersen, L. G. (1995) A Smooth Particle Mesh Ewald Method. *Journal of Chemical Physics* **103**, 8577-8593
84. Kabsch, W., and Sander, C. (1983) Dictionary of protein secondary structure: pattern recognition of hydrogen-bonded and geometrical features. *Biopolymers* **22**, 2577-2637
85. Laskowski, R. A., Rullmannn, J. A., MacArthur, M. W., Kaptein, R., and Thornton, J. M. (1996) AQUA and PROCHECK-NMR: programs for checking the quality of protein structures solved by NMR. *Journal of biomolecular NMR* **8**, 477-486
86. Koradi, R., Billeter, M., and Wuthrich, K. (1996) MOLMOL: a program for display and analysis of macromolecular structures. *Journal of molecular graphics* **14**, 51-55, 29-32

FOOTNOTES

This work was supported by a grant from the German Research Foundation to S.A.D. (DA 1195/3-2). S.A.D acknowledges further financial support from the Technische Universität München (TUM) diversity and talent management office by a Laura-Bassi award and the Helmholtz portfolio theme 'metabolic dysfunction and common disease' of the Helmholtz Zentrum München. M.S.A.R. is supported by the German Academic Exchange Service (DAAD) by a Ph.D. stipend. Work in DPT's group was supported by the Natural Sciences and Engineering Research Council of Canada. DPT is the Alberta Innovates Technology Futures Strategic Chair in (Bio)Molecular Simulation. Simulations were run on Compute Canada machines, supported by the Canada Foundation for Innovation and partners. This work was undertaken, in part, thanks to funding from the Canada Research Chairs program.

The abbreviations used are: ATM, ataxia telangiectasia mutated; ATR, ataxia- and Rad3-related; CMC, critical micelle concentration; DihepPC, 1,2-diheptanoyl-*sn*-glycero-3-phosphocholine; DMPC, 1,2-dimyristoyl-*sn*-glycero-3-phospho-choline; DNA-PKcs, DNA-dependent protein kinase catalytic subunit; DPC, dodecylphosphocholine; FATC, FRAP, ATM, TRRAP C-terminal; GB1, B1 immunoglobulin binding domain of streptococcal protein G (56 residues); hATMfatc-gb1ent, GB1 followed by a thrombin and an enterokinase recognition site (= LVPRGS-DDDDK) and residues 3024-3056 of human ATM; NOE, nuclear Overhauser effect; NOESY, NOE spectroscopy; PIKK, phosphatidylinositol-3 kinase-related kinase; (m)TOR, (mammalian/mechanistic) target or rapamycin; min, minute(s); SI, supplementary information; TOR, target of rapamycin; TRRAP, Transformation/transcription domain-associated protein.

Supporting Information

Superpositions of the spectra with and without $\{^1H\}$-^{15}N NOE of hATMfatc-gb1ent in the presence of 150 and 200 mM DPC and plots of the corresponding data as a function of the residue sequence position including for the 200 mM data also ^{15}N-T_1 and $-T_2$. Plots of the secondary structure content and the angles between helix 1 and 2 and 2 and 3 as a function of the simulation time, plots of global and local RMSF values, of the backbone and side chain RMSD, plots of the analysis of interhelical distances, the distance to the micelle center of mass and the SAS covered by DPC as a function of the residue sequence position, superpositions of the ^1H-^{15}N HSQC spectra of hATMfatc-gb1ent in the presence of 50 mM DPC and 1-4 mM 5- or 16-SASL, plots of 1-PRE values and the average chemical shift changes as a function of the residue sequence position for 1 and 2 mM 5- or 16-SASL data for

the whole hATMfatc-gb1ent, superpositions of the ^{1}H-^{15}N HSQC spectra of hATMfatc-gb1ent-F93/3049A and -W96/3052A in absence and presence of DPC or DihepPC micelles, DMPC/DihepPC bicelles or DMPC SUVs.

Table 1 Statistics for the 20 lowest energy NMR structures of the micelle-associated human ATM FATC domain (PDB-ID 6HKA)*	
Experimental restraints	
Distance restraints	All (assigned + ambiguous)
Total	748 (707 + 41)
^{15}N-NOESY	332 (313 + 19)
^{13}C-NOESY aliphatic / aromatic	366 (345 + 21) / 26 (25 + 1)
assigned short/medium/long range[§]	630/61/2
ambiguous short/medium/long range[§]	≤62/≤17/≤3
hydrogen bond	24
ϕ + ψ angle restraints	39
Structural statistics*	
RMSDs from experimental restraints	
Distance (Å)	0.0240±0.0030
Dihedral angle (°)	0.1937±0.1399
RMSDs from idealized geometry	
Bonds (Å)	0.0032±0.0002
Angles (°)	0.3709±0.0177
Improper (°)	0.2409±0.0145
Lennard-Jones energy (kcal mol^{-1})[$]	-141±31
Procheck (85) Statistics[#]	
Residues in most favored regions (%)	85.5
Residues in additional allowed regions (%)	14.5
Residues in generously allowed regions (%)	0.0
Residues in disallowed regions (%)	0.0
Average RMSD to mean structure	
Residues 70/3026-100/3056 (backbone/heavy) (Å)	4.47/5.26
Residues 73/3029-83/3039 (backbone/heavy) (Å)	0.37 / 0.89
Residues 87/3043-99/3055 (backbone/heavy) (Å)	1.32 / 2.33
Residues 87/3043-91/3047 (backbone/heavy) (Å)	0.22 / 1.35
Residues 95/3051-99/3055 (backbone/heavy) (Å)	0.27 / 1.72

*None of the structures had distance restraints violations > 0.5 Å or dihedral angle violations > 5°, RMSD = root mean square deviation, PDB-ID 6HKA; [§] short: i, i or i±1, medium: i, i±2 or 3 or 4, long range: here only i, i±5, note for ambiguous restraints two options were taken into account, thus the ≤ before the given numbers; [$]Calculated for the full 100 residue protein hATMfatc-gb1ent, but residues 1-67 had not been restrained and thus should not contribute significantly to the calculation; [#]For the well structured regions 72-83, 86-92, 94-100.

Table 2 Summary of the NMR-monitored interaction analysis of mutant hATMfatc-gb1ent proteins with different neutral membrane mimetics

Mutation	DPC micelles (50 mM)	DihepPC micelles (50 mM)	DMPC/DihepPC bicelles, (q = 0.2, [DMPC] = 0.04 M, and [DihepPC] = 0.20 M, cL 15%)	DMPC SUVs (< 50 mM DMPC)
F93/3049A	+	+	+	+
W96/3052A	+	+	+	+
F93/3049A-W96/3052A	+	+	+	-

+ = strong spectral changes indicating an interaction with the respective membrane mimetic, - = no significant spectral changes/interaction.

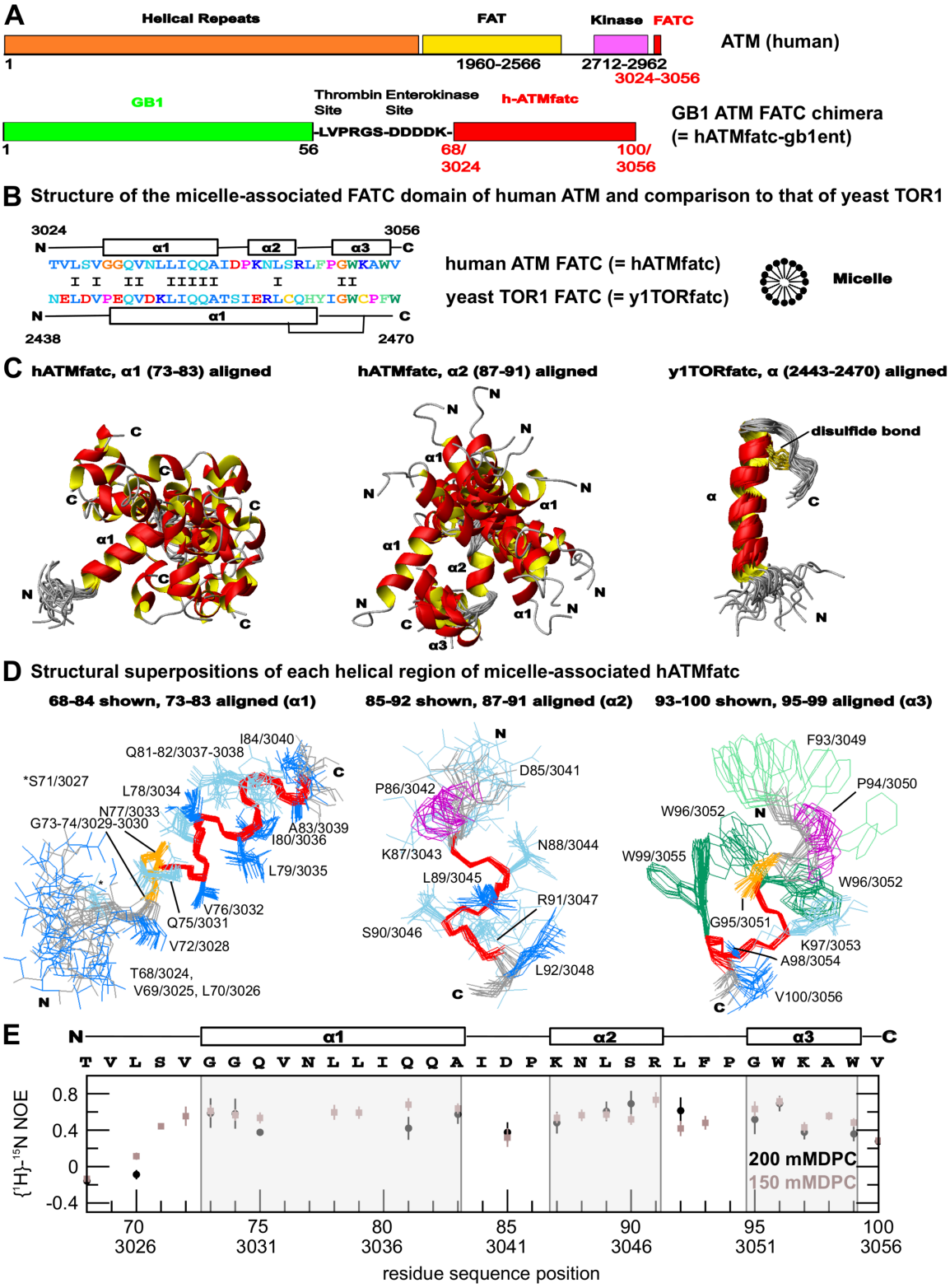

Fig. 1: NMR structure of the micelle-associated FATC domain of human ATM and comparison to that earlier determined for yeast TOR1. (A) Human ATM (hATM) consists of a long N-terminal region and a FAT domain, which are both made up of helical repeats, the catalytic Ser/Thr kinase domain, and the FATC domain (26). To structurally characterize the C-terminal FATC domain (residues 3024-3056, Uniprot-ID Q13315) it has been fused to the B1 domain of streptococcal protein G (GB1, 56 residues, = hATMfatc). B) Superposition of the amino acid sequences of the FATC

domains of hATM and yeast TOR1 and schematic representation of the secondary structure content in DPC micelles (schematic representation to the right). Aromatic residues are shown in light (F, H, Y) and dark (W) green, hydrophilic ones in light blue, except K and R in blue and D and E in red, and those containing methyl groups in dark blue. Prolines are colored purple and glycines (G2465) in orange. (C) The NMR structure of hATMfatc in the presence of micelles (150 mM DPC) consists of three helices with a central dynamic linker and a less dynamic C-terminal one (table 1, PDB-ID 6HKA, BMRB-ID 27167 (67)). The structure is overall different to that of the micelle-immersed oxidized yeast TOR FATC domain (y1fatc, PDB-ID 2KIO) (44). For the ribbon representations the 20 lowest energy structures have been superimposed for the indicated regions. (D) Each helical stretch of micelle-associated hATMfatc is shown in line mode. The backbone of the helical stretches is depicted in red. The color coding of the side chains is the same as in (B) except that charged side chains are also colored light blue. All structure pictures were made with the program MolMol (86). (E) Information about the backbone dynamics from a plot of the $\{^1H\}$-^{15}N NOE values of hATMfatc with 150 or 200 mM DPC as a function of the residue sequence position. No data can be obtained for prolines (86, 94) or overlapping peaks (SI Fig. S1). Values around 0.6-0.8 are typical for structured proteins. Lower NOE values indicate increased backbone flexibility. SI Fig. S1 shows the 2D $\{^1H\}$-^{15}N NOE and reference spectra and S2 additionally the ^{15}N-T_1 and -T_2 relaxation times at 200 mM DPC as well as a plot of the ^{15}N-relaxation data for the full hATMfatc-gb1ent fusion protein.

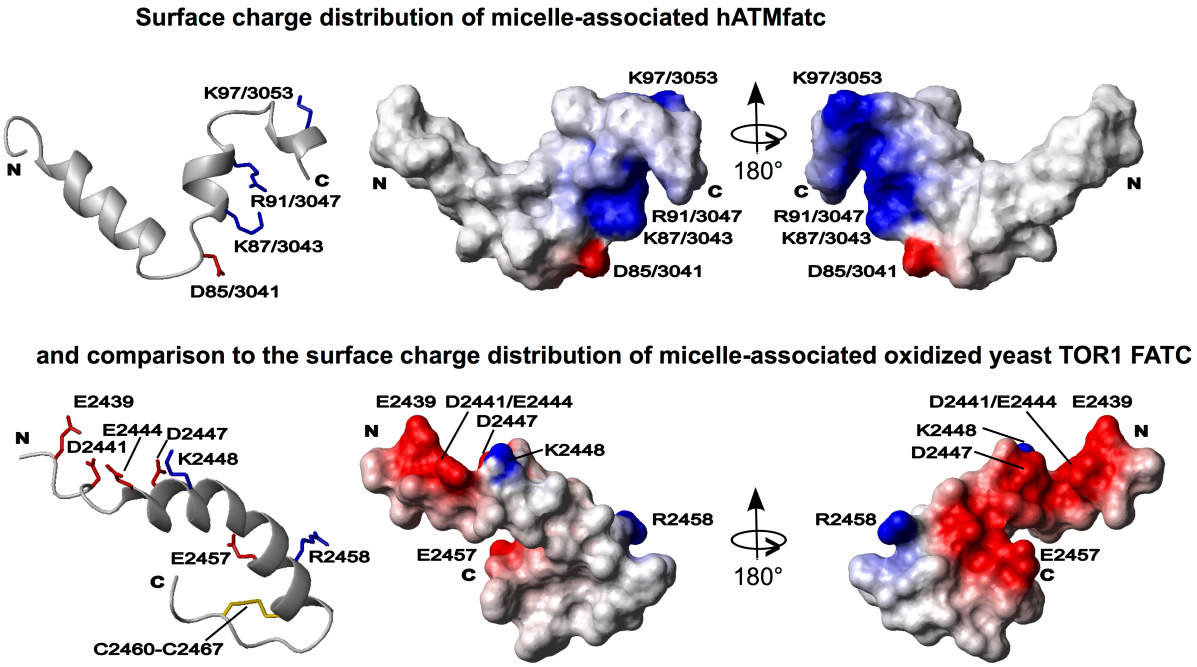

Fig. 2: The surface charge distribution of micelle-associated hATMfatc differs from that earlier determined for oxidized y1fatc (see also Fig. 1B-C) (44). Positively charged surface areas and side chains in stick mode in the ribbon representation are colored blue and negatively charged ones red. All structure pictures were made with the program MolMol (86).

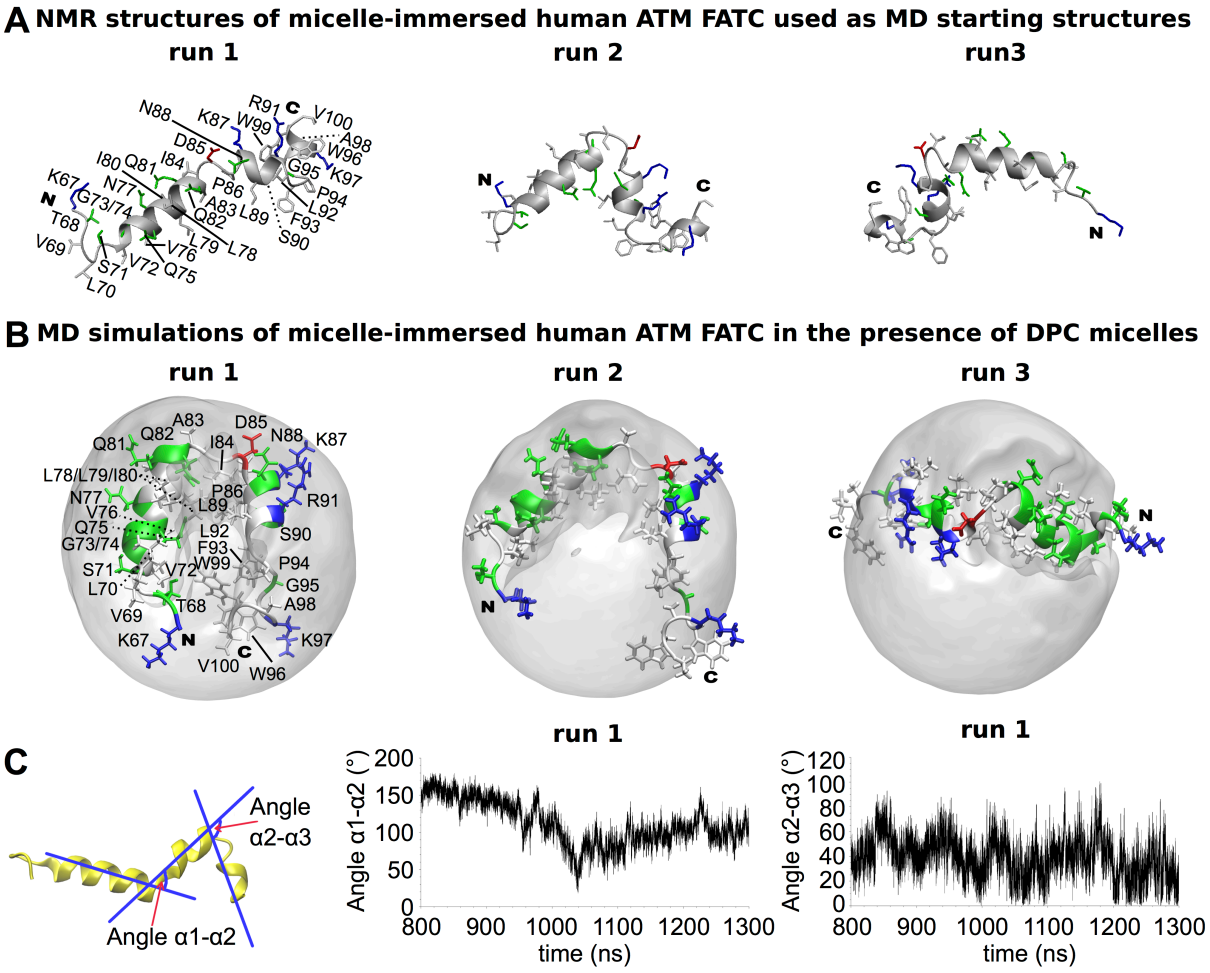

Fig. 3: Characterization of the dynamic properties of the micelle-associated FATC domain of human ATM (hATMfatc) from MD simulations. (A) Ribbon representations of the three lowest energy structures that were used as starting structures for three independent MD simulation runs. (B) Representative structure pictures of the MD simulations of hATMfatc in the presence of DPC micelles. The structures shown are the conformations of hATMfatc, which are the closest to the middle of the most populated cluster of structures for a given run. The DPC micelle is shown as a transparent averaged density iso-surface and the peptide in a ribbon representation. In both, (A) and (B), negatively charged side chains or residues are shown in red, positively charged ones in blue, polar ones in green and aliphatic ones in grey. For simplicity only the residue numbering as used in the pdb entry (PDB-ID 6HKA) is given. The N- and C-termini are indicated by the letters N and C. (C) Information about the movement of the 3 helices with respect to each other from an analysis of the variation of the angle between helix 1 and 2 as well as the one between helix 2 and 3 for run 1 (for runs 2 and 3 see SI Fig. S5A). Plots of the secondary structure content as a function of the simulation time are shown in SI Fig. S3. Plots the root mean square fluctuations (RMSF, global and local) and the backbone and side chain RMSD values as a function of the residue sequence position, a superposition of the top 10 cluster structures and an analysis of interhelical distances as a function of the simulation time are shown in SI Fig. S4.

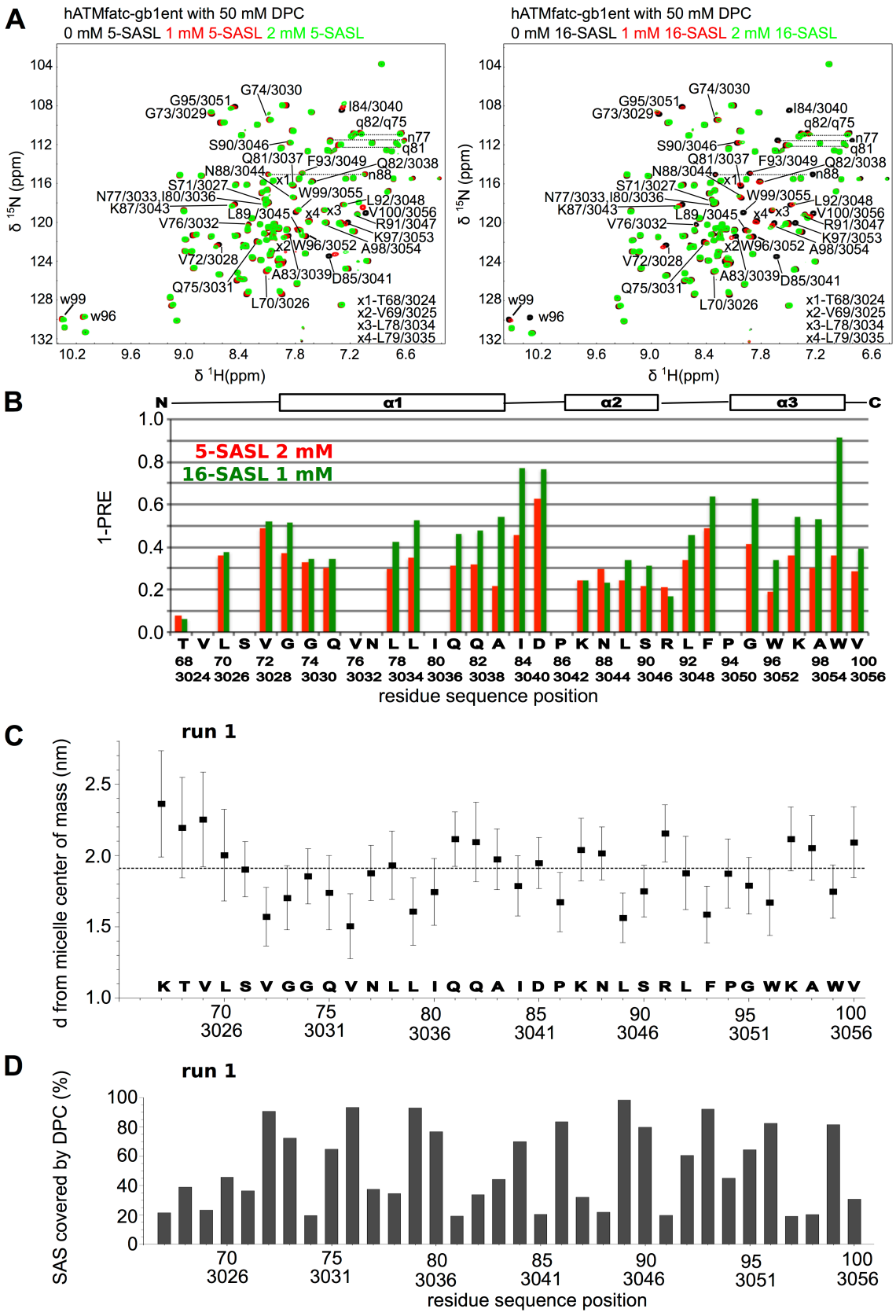

Fig. 4: Analysis of the membrane immersion properties of hATMfatc by NMR and MD simulations. (A) Superpositions of the ^{1}H-^{15}N HSQC spectra of hATMfatc-gb1ent in the presence of DPC micelles and 1 or 2 mM of paramagnetically tagged 5- (left) or 16- (right) doxyl stearic acid (5-/16-SASL, with

3 and 4 mM see SI Fig. S5B). The hATMfatc signals are labeled by the residue sequence position in hATMfatc-gb1ent/human ATM and the one letter amino acid code. The color coding is indicated at the top. (B) Diagrams of the paramagnetic relaxation enhancement (PRE) effects due to the presence of 5- or 16-SASL as a function of the residue sequence position. To better compare the PRE effects to the average chemical shift changes (SI Fig. S6, S7), 1-PRE (= 1- I(x mM SASL)/I (0 mM SASL)) was plotted. Accordingly, the larger the PRE effect, the higher the 1-PRE value. The sequence is given at the bottom and a schematic representation of the location of the helices at the top. (C) Diagram of the average distance of the center of mass (COM) of each residue of hATMfatc to that of the DPC micelle for run 1 (for runs 2 and 3 see SI Fig. S8). The averaging was performed over the last microsecond of the run. The dotted line corresponds to the average distance of the phosphor atom of the DPC head-group to the micelle COM (1.914 nm). (D) Diagram of the percentage of the solvent accessible surface area (SAS) of each residue of hATMfatc covered by DPC from run 1 (for runs 2 and 3 see SI Fig. S9). Residues with shorter distances to the micelle COM in (C) show usually a higher percentage in (D).

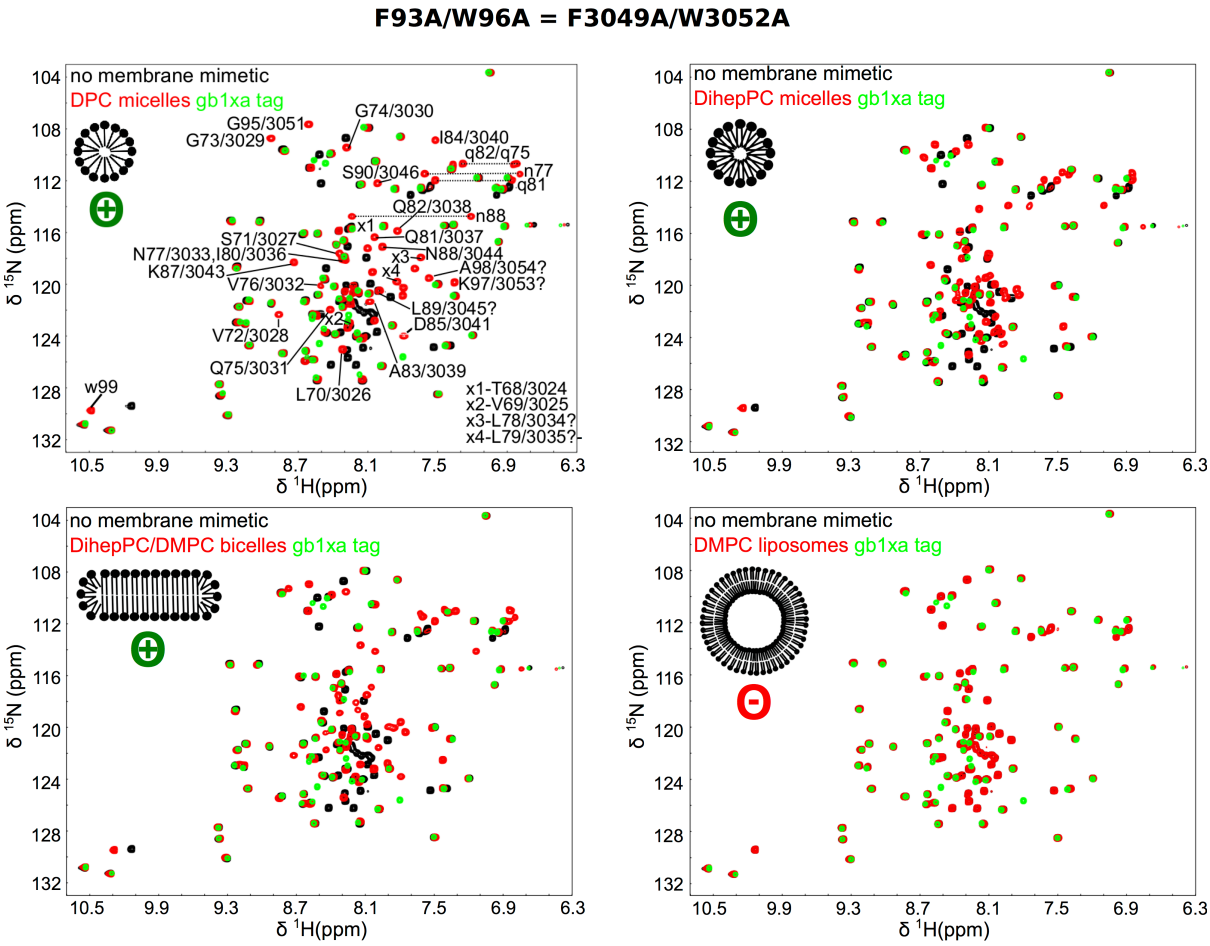

Fig. 5: Characterization of the role of conserved aromatic residues for the membrane affinity of hATMfatc. The pictures show superpositions of the ^{1}H-^{15}N HSQC spectra of the double mutant hATMfatc-gb1ent-F93/3049A-W96/3052A in the absence (black) and presence (red) of DPC micelles bicelles (q = 0.2, [DMPC] = 0.04 M, and [DihepPC] = 0.20 M, cL 15%, lower left) or DMPC liposomes (< 50 mM DMPC, lower right). Analogous superpositions for each single mutant (F93/3049A, W96/3052) are shown in SI Fig. S11C and S12B, respectively. A green plus below a schematic representation of the used membrane mimetic indicates strong spectral changes and thus interactions and a red plus no significant changes and thus no significant interactions. To better identify the signals of the ATM FATC part, the spectrum of the GB1 tag followed by a thrombin and

factor Xa site (= GB1xa) is additionally shown in green on top. Accordingly peaks with a green peak on top belong to the GB1 tag, which does not interact with membrane mimetics (41). In the spectrum in the presence of DPC, hATMfatc signals (red) are labeled by the 1-letter amino acid code and the sequence position based on similarity to the respective wild type spectrum. Small letters indicate side chain signals. A question mark behind the label indicates tentative assignments. Note that some red peaks that appear at new positions could not be assigned in this way and thus have no label. Superpositions of the ^{1}H-^{15}N HSQC spectrum of the wild type protein with that of each mutant are given in SI Fig. S10 and that in the presence of stepwise increasing concentrations of DPC for F93/3049A-W96/3052A in SI Fig. S11A, for F93/3049A in SI Fig. S11B and for W96/3052A in SI Fig. S12A.

NMR- and MD simulation–based structural characterization of the membrane-associating FATC domain of ataxia telangiectasia mutated

Munirah S. Abd Rahim, Yevhen K. Cherniavskyi, D. Peter Tieleman and Sonja A. Dames

J. Biol. Chem. published online March 13, 2019
